Earthq Eng & Eng Vib (2018) 17: 693-706 **DOI**: https://doi.org/10.1007/s11803-018-0469-2

Experimental and analytical study on design performance of full-scale viscoelastic dampers

Shiang-Jung Wang[1†], I-Chen Chiu[2‡], Chung-Han Yu[3§] and Kuo-Chun Chang[4*]

1. *Department of Civil and Construction Engineering, Taiwan University of Science and Technology, Taipei, Chinese Taipei*
2. *Department of Civil Engineering, Taiwan University (NTU), Taipei, Chinese Taipei*
3. *Center for Research on Earthquake Engineering (NCREE), Taipei, Chinese Taipei*
4. *Department of Civil Engineering, Taiwan University (NTU), Taipei, Chinese Taipei*

Abstract: Viscoelastic (VE) dampers, with their stiffness and energy dissipation capabilities, have been widely used in civil engineering for mitigating wind-induced vibration and seismic responses of structures, thus enhancing the comfort of residents and serviceability of equipment inside. In past relevant research, most analytical models for characterizing the mechanical behavior of VE dampers were verified by comparing their predictions with performance test results from small-scale specimens, which might not adequately or conservatively represent the actual behavior of full-scale dampers, especially with regard to the ambient temperature, temperature rise, and heat convection effects. Thus, in this study, by using a high-performance testing facility with a temperature control system, full-scale VE dampers were dynamically tested with different displacement amplitudes, excitation frequencies, and ambient temperatures. By comparing the analytical predictions with the experimental results, it is demonstrated that adopting the fractional derivative method together with considering the effects of excitation frequencies, ambient temperatures, temperature rises, softening, and hardening, can reproduce the design performance of full-scale VE dampers very well.

Keywords: viscoelastic damper, full-scale, design performance, dynamic test, fractional derivative model

1 Introduction

In addition to the basic need for protecting life safety, performance-based seismic design (Ghobarah, 2001) emphasizes the importance of reducing repair efforts and costs for structural and nonstructural components after frequent earthquakes as well as preventing equipment inside the structure from malfunction during earthquakes, which could significantly affect life, safety and cause major economic losses. To decrease the input energy caused by earthquakes directly transmitted to the to-be-protected structure and thus meet the performance-based design goals, the incorporation of supplemental energy dissipation systems into structures (Soong and Spencer, 2002) has been regarded as one of the most effective and feasible strategies. In other words, supplemental dampers play an important role in the first line of defense against seismic impact on the installed structures as well as the people and equipment inside. By doing so, frequent damage to structures due to their inelastic deformation (or ductile behavior) can be avoided, and acceleration responses can be well controlled to guarantee daily functions of important equipment and ensure the comfort of people inside them.

Among the velocity-type dampers (Soong and Spencer, 2002), viscoelastic (VE) dampers feature stiffness and energy dissipation capabilities through the shear deformation of polymer composite (termed as VE) material layers sandwiched between steel plates (Chang *et al*., 1993). The force capacity can be easily increased by designing multiple VE material layers in parallel. Different from fluid dampers such as viscous dampers or oil dampers (Soong and Spencer, 2002), VE dampers composed of VE material layers and steel plates are very simple in mechanism. Their inherent stiffness can provide additional resisting (or restoring) force, and most importantly, they avoid the problem of liquid leakage. In addition, since VE dampers are usually designed as a panel (or wall) type, their installation in a building structure is very easy, can architecturally meet opening requirements, and can be easily incorporated into interior design by using partition walls, which are attractive to

Correspondence to: Kuo-Chun Chang, Department of Civil Engineering, Taiwan University (NTU), Taipei, Chinese Taipei
Tel: +886-2-33664232; Fax: +886-2-27396752
E-mail: ciekuo@ntu.edu.tw
†Associate Professor; ‡Graduate Student; §Assistant Researcher; *Professor
Supported by: Science and Technology Authority of Taiwan under Grant No.107-2221-E-492-004-
Received August 8, 2018; **Accepted** September 21, 2018

architects and owners. Due to these advantages, VE dampers have been widely used in civil engineering throughout the world for a variety of purposes (Samali and Kwok, 1995). In the beginning, they were used for mitigating the wind-induced vibration of high-rise buildings, such as the twin towers of the World Trade Center buildings in New York City (Mahmoodi *et al*., 1987) and the Columbia Seafirst building in Seattle, Washington (Skilling *et al*., 1986). Subsequently, they were adopted to enhance the seismic performance of buildings (Chang *et al*., 1993). In Taiwan, to date, the number of new and retrofitted buildings installed with VE dampers exceeds 150 (Wang *et al*., 2017).

Since the 1990s, a large number of studies on VE dampers for seismic application have been launched. With regard to performance tests on VE material, Chang *et al*. (1992) conducted cyclic loading tests on small-scale VE dampers to obtain their force-deformation relationship and their dependence on shear strains, excitation frequencies, and ambient temperatures. Kasai *et al*. (1993, 2001) and Kasai and Tokoro (2002) conducted a series of performance tests on small-scale VE dampers to thoroughly examine their dependence on excitation frequencies, ambient temperatures, and temperature rises as well as their softening and hardening behavior. Bergman and Hanson (1993) examined the influence of excitation frequencies, displacement amplitudes, temperatures, and cumulative energy absorption on the mechanical properties and hysteretic stability of VE dampers by testing small-scale specimens. Lai *et al*. (1995) performed free- and forced- vibration tests on small-scale VE dampers. Xu *et al*. (2015) performed cyclic loading tests on small-scale VE dampers with different excitation frequencies and displacement amplitudes. De Lima *et al*. (2015) experimentally studied the self-heating effect of small-scale VE dampers under static and dynamic loadings.

With performance test verification of small-scale specimens, different approaches for mathematically modeling the force-deformation (or stress-strain) relationship of VE dampers (or material) have been presented. Gemant (1936) adopted the fractional derivative method to characterize the frequency-dependent behavior of VE material. Bagley and Torvic (1983) used fractional calculus to construct the stress-strain relationship of VE material and analyzed a viscoelastically damped structure model. Kasai *et al*. (1993, 2001) and Kasai and Tokoro (2002) proposed an advanced model for VE dampers which can incorporate the effects of excitation frequencies, ambient temperatures, temperature rises, softening, and hardening into the fractional derivative model. Shen and Soong (1995) developed an analytical model for predicting the hysteretic behavior of VE dampers based on Boltzmann's superposition principle and the method of reduced variables. The proposed model was also compared with the fractional derivative one. Aprile *et al*. (1997) proposed an evolutionary model to describe the dependence of mechanical properties of VE dampers on deformation frequencies and temperature increases respectively by using the fractional derivative operators and the evolutionary transfer function. Xu *et al*. (2015) proposed an equivalent fractional Kelvin model for VE dampers which can further take temperature and frequency effects into consideration. Lewandowski and Chorążyczewski (2010) presented a family of methods for identifying the parameters of the Kelvin–Voigt and Maxwell fractional models. Gandhi and Chopra (1996) developed a viscoelastic solid model comprising linear and nonlinear springs together with dashpots to represent the dynamic behavior of VE dampers. The analytical results of VE dampers obtained by the fractional derivative method and standard mechanical model consisting of springs and dashpots were compared by Park (2001). Chang and Singh (2009) provided explicit steps and necessary formulas to represent the frequency-dependent characteristics of VE dampers by using the storage and loss modulus in the two classical models.

From past relevant research, it can be found that the applicability of most analytical models for characterizing the mechanical behavior of VE dampers were verified through the comparison with performance test results of small-scale specimens. To prove that adopting the fractional derivative method together with considering the effects of excitation frequencies, ambient temperatures, temperature rises, softening, and hardening can still wellrepresent the design performance of full-scale VE dampers, two full-scale specimens were dynamically tested by using the high-performance damper testing facility at the Taipei Laboratory of the Center for Research on Earthquake Engineering (NCREE) (Wang *et al*., 2017) in this study. Different test conditions, including different displacement amplitudes, excitation frequencies, and ambient temperatures, are considered in the scheme.

2 Experimental study

2.1 Test specimens and setup

Two full-scale VE dampers, denoted as Specimens A and B herein, manufactured by the Nippon Steel & Sumitomo Metal Corporation (http://www.nssmc.com/) are chosen as the test specimens in this study, as shown in Fig. 1. Each damper comprises four VE material layers (Type ISD111 (http://www.nssmc.com/)) of thickness 5 mm each and square area of 2500 cm^2 each. The four VE material layers are designed in parallel and are sandwiched in between five steel plates, as shown in

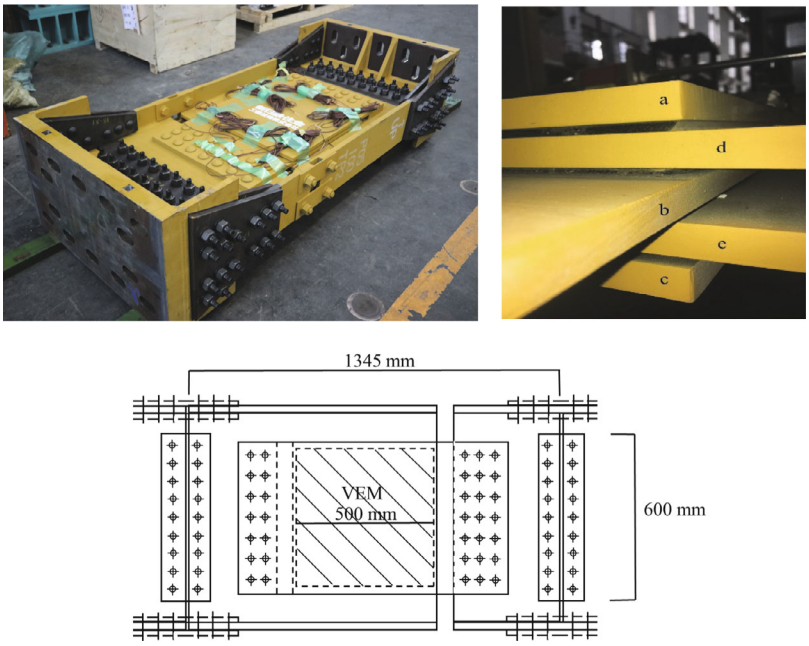

Fig. 1 VE damper specimens

Fig. 1. The nominal shear force capacity of each damper is designed to be 500 kN. At one end of the three steel plates (i.e. a, b, and c plates as denoted in Fig. 1) and at the other end of the rest (i.e., d and e plates as denoted in Fig. 1), additional steel components are designed with bolt joints for compactly connecting the VE damper body with the testing facility (or with the structure in engineering practice).

By using the high-performance damper testing facility at the NCREE Taipei Laboratory (Wang *et al.*, 2017) , the VE damper specimens were dynamically tested subjected to uniaxial reversal loading, as shown in Fig. 2. The testing facility consists of three steel reaction components, a temperature control system, and a high-speed servo-hydraulic actuator that possesses a maximum stroke capacity of ±600 mm and a maximum force capacity of ±2 MN. The maximum velocity capacity is ±1 m/s when the force reaches ±1 MN. Pre-stressed steel bars are employed to mount the three reaction components on the strong floor as well as assemble the actuator, reaction components, and any necessary fixtures. The reaction component connected to the actuator piston end is designed with a linear guide system, thus guaranteeing a nearly perfect uniaxial movement control with very limited friction force. Test specimens are installed horizontally at the space between the two reaction components, which can be adequately adjusted to comply with different size requirements. With the temperature control system, the ambient and operating temperatures of the specimens varying from 5°C to 50°C can be controlled and monitored in the chamber.

2.2 Test protocols and measurement sensors

Specimens A and B were tested under a series of sinusoidal reversal loading with different excitation frequencies varying from 0.1 Hz to 5 Hz, ambient

Fig. 2 Test installation

temperatures varying from 10°C to 40°C (i.e. the normal temperature variation in Taiwan) with an increment of 10°C, and maximum shear strains (γ_{max}) varying from 60% to 300%. The VE damper specimens, basically, should remain intact without any damage after completing all the tests. In other words, the nominal design range of the specimens should be larger than 300% shear strain. Note that under a specific shear strain and at a specific ambient temperature, the excitation frequency was not further increased when the measured maximum shear force exceeded 800 kN. There are six cycles for each test condition. The test program is detailed in Table 1.

In addition to the built-in displacement transducer and load cell of the high-speed servo-hydraulic actuator for recording the test results, an additional linear variable differential transformer (LVDT) was installed on the VE damper specimens to measure their pure shear deformation (i.e. excluding any deformation induced by other components, connections, fixtures, and etc. as well as any gaps) during the tests, as shown in Fig. 3(a). One thermocouple, denoted as T_a in Fig. 3(b), was used in the air to measure the ambient temperature during the tests. To clarify the temperature sensitivity of the VE material, as well as to correct the analytical model in consideration of the temperature rise effect, ten thermocouples, denoted as T_{1A}, T_{1B}, T_{1C}, T_{1D}, T_{1E}, T_{2A}, T_{2B}, T_{2C}, T_{2D}, and T_{2E} in Fig. 3(b), were embedded in the first and second VE material layers with a symmetric plane arrangement (five in each layer). In addition, another thermocouple, denoted as T_s in Fig. 3(b), was attached on the top steel plate. Therefore, during and after the tests, the schematic temperature distribution contours in the VE material layers, together with the heat convection from the VE material layers to the top steel plate, can be experimentally examined. The sampling rate for data acquisition is 1 Hz.

2.3 Test results and discussion

The experimental force-displacement relation of Specimens A and B under a maximum shear strain of 60% with various excitation frequencies and at different ambient temperatures is shown in Fig. 4. The average shear storage stiffness $K_{d,avg}$, the average damping coefficient $C_{d,avg}$, and the average maximum shear force response $F_{max,avg}$ considering the test data of the intermediate five complete cycles (i.e. excluding the beginning half and ending half cycles), as calculated in Eqs. (1) to (3) (FEMA 273, 1997) respectively, are summarized in Table 2. As observed from the figure and table, with the same maximum shear strain, a higher excitation frequency (or strain rate) will lead to a larger shear storage stiffness and a smaller damping coefficient but a larger hysteretic loop area. The higher the ambient temperature, the smaller the shear storage stiffness, damping coefficient, and hysteretic loop area.

Table 1 Test protocols of two VE damper specimens

	Specimen	A	B
Sinusoidal reversal loading	Excitation frequency (Hz)	0.1, 0.2, 0.3, 0.35, 0.4, 0.45, 0.5, 0.65, 0.85, 1, 1.5, 2, 3, 4, 5	
	Maximum shear strain (%)	60, 100, 200, 300	
	Ambient temperature (°C)	10, 20, 30, 40 (±2°C tolerance)	
	Number of cycles	6	

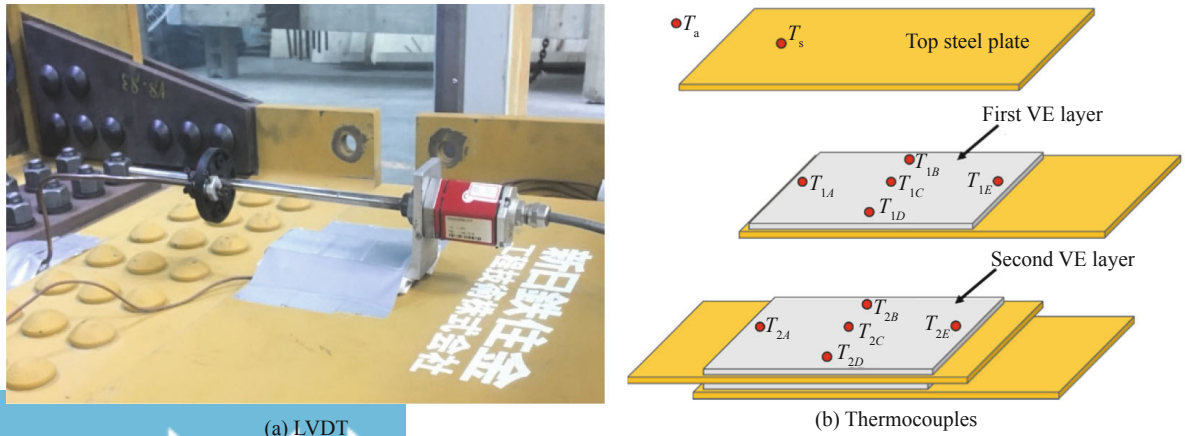

(a) LVDT (b) Thermocouples

Fig. 3 Layouts of measurement sensors

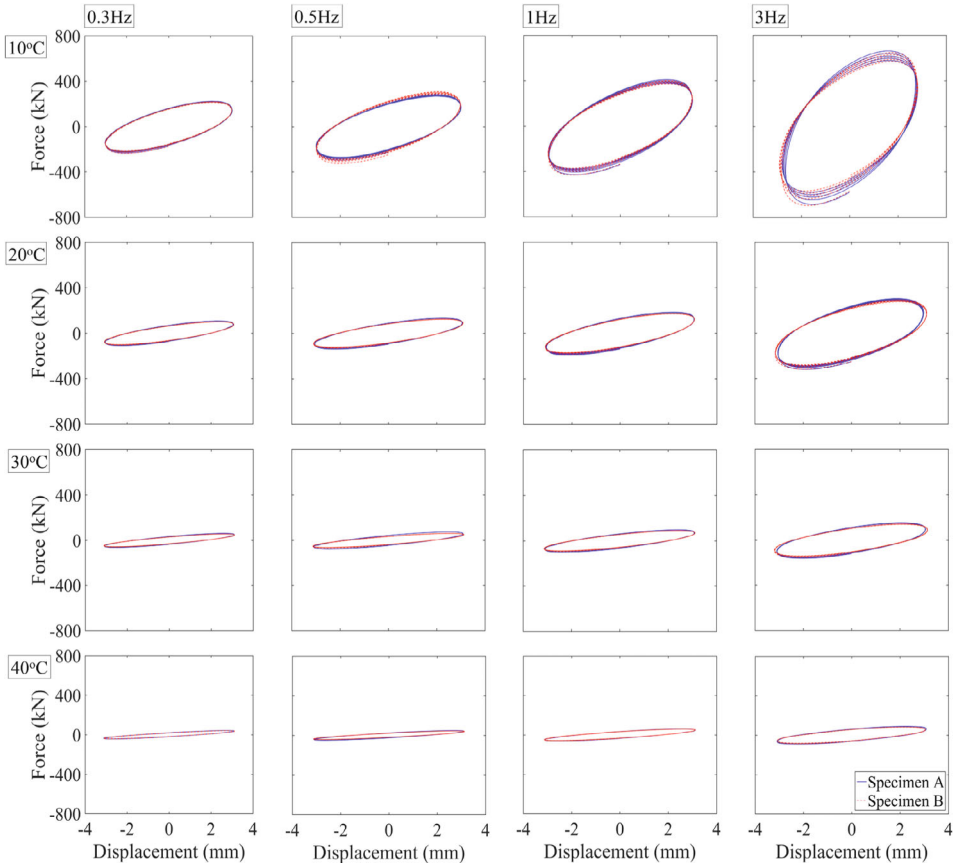

Fig. 4 Experimental force-displacement relation of Specimens A and B under 60% shear strain with various excitation frequencies and at different ambient temperatures

Table 2 Comparison of calculated characteristics

Excitation frequency (Hz)		0.3	0.3	0.3	0.3	0.5	1
Ambient temperature (°C)		10	20	30	40	20	20
Maximum shear strain (%)					60		
$K_{d,\,avg}$ (kN/mm)	Specimen A (1)	47.81	25.15	15.72	11.59	29.77	39.55
	Specimen B (2)	48.77	24.59	14.99	11.51	29.40	39.52
Difference (%)	$[(2)-(1)]/(1)\times 100\%$	2.01	-2.22	-4.65	-0.69	-1.26	-0.09
$C_{d,\,avg}$ (kN·s/mm)	Specimen A (3)	28.31	12.11	5.79	3.34	9.53	6.88
	Specimen B (4)	27.79	11.09	5.10	3.12	8.74	6.35
Difference (%)	$[(4)-(3)]/(3)\times 100\%$	-1.85	-8.44	-12.01	-6.49	-8.33	-7.66
$F_{max,\,avg}$ (kN)	Specimen A (5)	222.90	107.86	61.64	42.64	134.98	184.32
	Specimen B (6)	222.09	102.08	56.81	41.01	125.64	175.19
Difference (%)	$[(6)-(5)]/(5)\times 100\%$	-0.37	-5.36	-7.83	-3.83	-6.92	-4.95

In addition, with a tolerance of ±2°C for controlling the target ambient temperature when testing the two specimens, the differences between the obtained mechanical properties of Specimens A and B are very limited and remain within an acceptable range.

$$K_{d,\,avg}=\frac{1}{5}\left(\sum_{i=1}^{5}\frac{\left|F_i^+\right|+\left|F_i^-\right|}{\left|d_i^+\right|+\left|d_i^-\right|}\right) \tag{1}$$

$$C_{\mathrm{d,\,avg}}=\frac{1}{5}\left\{\sum_{i=1}^{5}\frac{W_{D,\,i}}{\pi\omega\left[\left(\left|d_i^{+}\right|+\left|d_i^{-}\right|\right)/2\right]^2}\right\} \tag{2}$$

$$F_{\mathrm{max,\,avg}}=\frac{1}{5}\left(\sum_{i=1}^{5}\frac{\left|F_{i,\,\mathrm{max}}^{+}\right|+\left|F_{i,\,\mathrm{min}}^{-}\right|}{2}\right) \tag{3}$$

where d_i^{+} and d_i^{-} are the positive maximum and negative minimum shear deformation measured at the ith cycle (excluding the beginning half and ending half cycles) of loading, respectively; F_i^{+} and F_i^{-} are the measured shear forces at d_i^{+} and d_i^{-}, respectively; $W_{D,\,i}$ is the calculated enclosed hysteresis loop area at the ith cycle of loading; ω is the angular frequency of sinusoidal reversal loading; and $F_{i,\,\mathrm{max}}^{+}$ and $F_{i,\,\mathrm{min}}^{-}$ are the positive maximum and negative minimum shear forces measured at the ith cycle of loading.

The experimental force-displacement relation of Specimen A under maximum shear strains varying from 60% to 300% with two excitation frequencies, 0.3 Hz and 0.85 Hz, and at an ambient temperature of 20°C is shown in Fig. 5. In addition to $K_{\mathrm{d,\,avg}}$ and $C_{\mathrm{d,\,avg}}$ calculated from the intermediate five-cycle test data, the maximum shear force response obtained from the beginning half cycle, $F_{\mathrm{max,\,beginning}}$, is given in the figure for comparison purposes. As observed from the figure and calculated characteristics, the shear storage stiffness and damping coefficient are reduced as the shear strain increases, which is the so-called softening phenomenon. By comparing Figs. 5(a) and 5(b), the shear force amplification at the beginning half cycle becomes more significant when subjected to a higher shear strain (or more precisely, a higher strain rate). This is attributed to the hardening effect.

The measurement from T_{2C} of Specimen A, as shown in Fig. 3(b), under maximum shear strains varying from 60% to 300% with an excitation frequency of 0.65 Hz and at an ambient temperature of 20°C is presented in Fig. 6(a). The measurement from T_{2C} of Specimen A under a maximum shear strain of 300% with another two excitation frequencies, 0.2 Hz and 0.4 Hz, is also provided in the figure. Obviously, the temperature rise within the VE material reaches the maximum when ending the external disturbance. Afterward, the temperature is lowered through conduction and radiation and then gradually returns to be approximately identical to the ambient temperature. It can be seen that the larger the shear strain and strain rate are (or more precisely, the larger the hysteretic loop area), the higher the temperature rise within the VE material, resulting in a longer cooling time. Figure 6(b) presents the temperature distribution contours of the five thermocouples embedded in the first and second VE material layers of Specimen A at the instant of 24 seconds after starting the test under a maximum shear strain of 300% with an excitation frequency of 0.65 Hz and at an ambient temperature of 20°C. Apparently, at the same instant, the temperature measured in the first VE material layer is lower than that in the second layer and is closer to the ambient temperature. This is reasonable because the top steel plate adjacent to the first VE material layer has much more radiation area directly in contact with the air, thus it has better heat radiation efficiency. Meanwhile, the temperatures measured at the edge of the two VE material

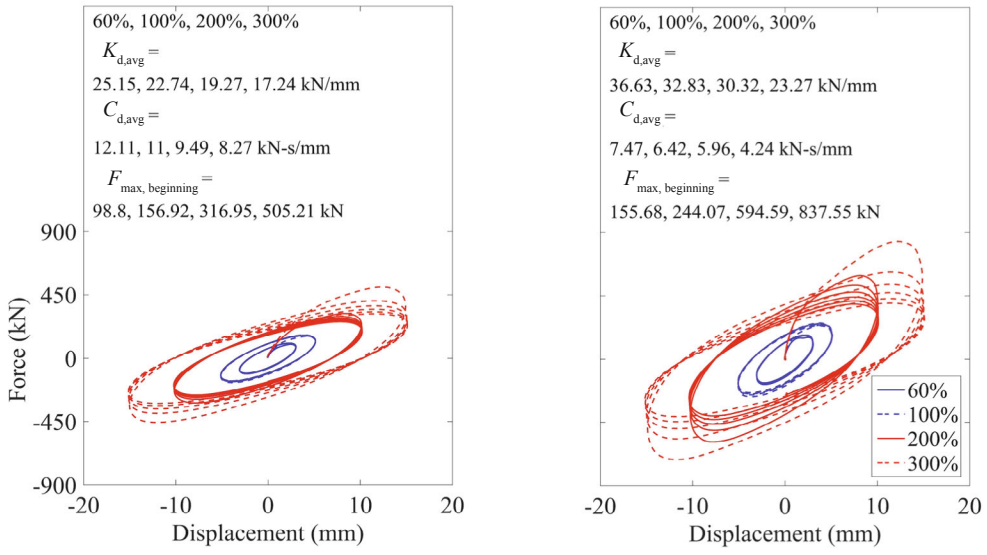

(a) Excitation frequency: 0.3 Hz (b) Excitation frequency: 0.85 Hz

Fig. 5 Experimental force-displacement relation of Specimen A under shear strains not greater than 300% and at 20°C

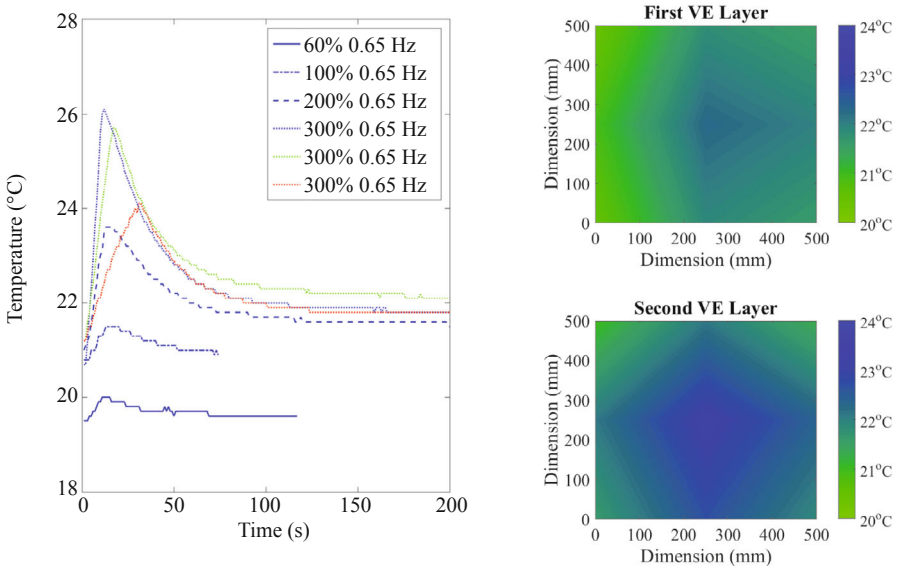

(a) Time histories of temperature variation (b) Temperature distribution contours (24 seconds after starting)

Fig. 6 Temperature rises and cooling of VE material of Specimens A and B respectively during and after tests

layers (i.e. measurement from T_{1A}, T_{1B}, T_{1D}, T_{1E}, T_{2A}, T_{2B}, T_{2D}, and T_{2E} as shown in Fig. 3(b)) are lower than those at the center (i.e. measurement from T_{1C} and T_{2C} as shown in Fig. 3(b)) because of their shorter path to the VE material surfaces directly in contact with the air.

Basically, Specimen B has the same tendencies in terms of mechanical properties and temperature variation as those observed from Specimen A as presented in Figs. 5 and 6.

3 Analytical model

3.1 Excitation frequency effect

Gemant (1936) first applied the fractional derivative method to characterize the frequency-dependent behavior of VE material. Afterward, this method has been widely adopted in analytical and numerical research relevant to VE dampers. Its general form is expressed as

$$\tau(t)+\sum_{i=1}^{M}a_i D^{\alpha_i}\left[\tau(t)\right]=G\left\{\gamma(t)+\sum_{j=1}^{N}b_j D^{\beta_j}\left[\gamma(t)\right]\right\} \quad (4)$$

where $\tau(t)$ and $\gamma(t)$ are the shear stress and strain at time t respectively; M and N are the total numbers of stress and strain terms in the summation, respectively; a_i, α_i and b_j, β_j are the to-be-determined coefficients of the ith stress term and jth strain term that are required to be identified from test results, respectively, and note that $0<\alpha_i, \beta_j<1$; G is the shear modulus that are required to be identified from test results; and D is the differential operator. The fractional derivative calculus with a power of n ($0< n <1$) for a function $\gamma(t)$ is defined as

$$D^n\left[y(t)\right]=\frac{1}{\Gamma(1-n)}\frac{\mathrm{d}}{\mathrm{d}t}\int_0^t\frac{y(x)}{(1-x)^n}\mathrm{d}x \quad (5)$$

where Γ is the Gamma function and x is a dummy variable.

By taking $M=N=1$ in Eq. (4), a simpler form of the fractional derivative model with five to-be-determined coefficients, a_1, α_1, b_1, β_1, and G, can be derived as given in Eq. (6) (Bagley and Torvic, 1983). Note that the subscripts of a_1, α_1, b_1, and β_1 are omitted and these coefficients are replaced by a, α, b, and β, respectively, for a simpler expression. By letting $\alpha=\beta$ in Eq. (6), a further simplified form with four to-be-determined coefficients, a, α, b, and G, can be obtained as given in Eq. (7) (Kasai *et al.*, 1993). By setting $a=0$ in Eq. (6), the simplest form with three to-be-determined coefficients, b, β, and G, can be obtained as given in Eq. (8).

$$\tau(t)+aD^{\alpha}\left[\tau(t)\right]=G\left\{\gamma(t)+bD^{\beta}\left[\gamma(t)\right]\right\} \quad (6)$$

$$\tau(t)+aD^{\alpha}\left[\tau(t)\right]=G\left\{\gamma(t)+bD^{\alpha}\left[\gamma(t)\right]\right\} \quad (7)$$

$$\tau(t)=G\left\{\gamma(t)+bD^{\beta}\left[\gamma(t)\right]\right\} \quad (8)$$

The further simplified form of the fractional derivative model as given in Eq. (7) is adopted in this study. By performing Fourier transform on Eq. (7),

recognizing that the shear stress $\tau(t)$ of VE dampers can be expressed as Eq. (9) (Chang *et al*., 1993), and comparing the coefficients in the real and imaginary parts, the shear storage modulus $G'(\omega)$ with four to-be-determined coefficients, *a*, *α*, *b*, and *G*, and the loss factor $\eta(\omega)$ $(=G''(\omega)/G'(\omega))$ with three to-be-determined coefficients, *a*, *α*, and *b*, can be obtained as given in Eqs. (10) and (11), respectively.

$$\tau(t)=G^*(\omega)\gamma(t)=\left[G'(\omega)+\mathrm{i}G''(\omega)\right]\gamma(t)= G'(\omega)\left[1+\mathrm{i}\eta(\omega)\right]\gamma(t) \tag{9}$$

$$G'(\omega)=G\frac{1+ab\omega^{2\alpha}+(a+b)\omega^{\alpha}\cos(\alpha\pi/2)}{1+a^2\omega^{2\alpha}+2a\omega^{\alpha}\cos(\alpha\pi/2)} \tag{10}$$

$$\eta(\omega)=\frac{(-a+b)\omega^{\alpha}\sin(\alpha\pi/2)}{1+ab\omega^{2\alpha}+(a+b)\omega^{\alpha}\cos(\alpha\pi/2)} \tag{11}$$

where $G'(\omega)$ is the shear storage modulus; $G''(\omega)$ is the shear loss modulus; $\eta(\omega)$ is the loss factor; $G^*(\omega)$ is the shear modulus in a complex form; and ω is the angular frequency.

The shear storage modulus and loss factor of VE dampers considering the frequency effect can be calculated by using a series of sinusoidal reversal loading test results with different excitation frequencies. Therefore, by adopting the least squares method as given in Eq. (12), the values of the coefficients *a*, *α*, and *b* can be determined first. Then, with known *a*, *α*, and *b*, the value of the coefficient *G* can be determined as given in Eq. (13).

$$\min\left\{\sum_{i=1}^{n}\left[\eta(a,\ \alpha,\ b,\ \omega_i)-\eta_i\right]^2\right\} \tag{12}$$

$$\min\left\{\sum_{i=1}^{n}\left[G'(G,\ \omega_i)-G'_i\right]^2\right\} \tag{13}$$

where ω_i $(i=1\text{ to }n)$ is the *i*th angular frequency of sinusoidal reversal loading tests (*n* sets of different angular frequencies are considered); G'_i and η_i are the experimental shear storage modulus and loss factor of VE dampers under sinusoidal reversal loading with an angular frequency of ω_i at the reference temperature T_{ref}; and $\eta(a,\ \alpha,\ b,\ \omega_i)$ and $G'(G,\ \omega_i)$ are calculated as per Eqs. (11) and (10), respectively, on the premise that the determined values of the coefficients *a*, *α*, *b*, and *G* can satisfy Eqs. (12) and (13).

3.2 Ambient temperature effect

The so-called "Temperature-Frequency Equivalence Property" (Kasai *et al*., 2001; Kasai and Tokoro, 2002) has been frequently adopted in many past research studies to describe the ambient temperature-dependent property of VE material. By means of a shift factor λ which is a function of the ambient temperature considered T_{amb} as given in Eq. (14), the forms of the coefficients *a* and *b* at T_{amb} can be represented by Eqs. (15) and (16), respectively. In other words, $\lambda\omega$, instead of ω, is substituted into Eqs. (10) and (11) to represent the shear storage modulus and loss factor at T_{amb}.

$$\lambda=\exp\left[-p_1\left(T_{\mathrm{amb}}-T_{\mathrm{ref}}\right)/\left(p_2+T_{\mathrm{amb}}-T_{\mathrm{ref}}\right)\right] \tag{14}$$

$$a=a_{\mathrm{ref}}\lambda^{\alpha} \tag{15}$$

$$b=b_{\mathrm{ref}}\lambda^{\alpha} \tag{16}$$

where p_1 and p_2 are the constants that are required to be determined by test measurement at T_{amb}; and a_{ref} and b_{ref} are the determined values of the coefficients *a* and *b* in Eq. (7) at T_{ref}, respectively.

Through the least squares method as given in Eq. (17), the constants p_1 and p_2 can be determined.

$$\min\left\{\sum_{i=1}^{n}\left\{\left[G'_{\mathrm{ref}}(\lambda\omega_i)-G'_i\right]^2+\left[\eta_{\mathrm{ref}}(\lambda\omega_i)-\eta_i\right]^2\right\}\right\} \tag{17}$$

where G'_i and η_i are the experimental shear storage modulus and loss factor of VE dampers under sinusoidal reversal loading with an angular frequency of ω_i at T_{amb}, respectively; and $\eta_{\mathrm{ref}}(\lambda\omega_i)$ and $G'_{\mathrm{ref}}(\lambda\omega_i)$ are calculated as per Eqs. (11) and (10), respectively, on the premise that the determined values of the coefficients a $(=a_{\mathrm{ref}}\lambda^{\alpha})$ and b $(=b_{\mathrm{ref}}\lambda^{\alpha})$ can satisfy Eq. (17).

3.3 Temperature rise effect

Under external excitation, the energy absorbed or dissipated by VE material through its deformation (shear deformation in general) will be transformed into the form of heat, thus causing the temperature rise within the VE material. When VE dampers installed in structures are subjected to short duration loading, such as ground shaking caused by earthquakes, their temperature rise in a short period of time was studied (Kasai *et al*., 2001; Kasai and Tokoro, 2002) and can be rationally estimated by

$$T(t)=T_0+\frac{1}{s\rho}\int\tau(t)\mathrm{d}\gamma(t) \tag{18}$$

where T_0 is the initial ambient temperature; $T(t)$, *s*, and ρ are the temperature at time *t* under excitation, specific heat, and mass density of the VE material, respectively.

The thermal energy within the VE material, of course, will be conducted and radiated through the contact steel

plates and air, respectively. After the external disturbance is terminated, the temperature of the VE material will be lowered with time and gradually return to be the same as the ambient temperature. The temperature decreasing rate at time t, $\mathrm{d}T(t)/\mathrm{d}t$, can be estimated by a higher-order polynomial function of $\Delta T(t)$ (Kasai *et al.*, 2001; Kasai and Tokoro, 2002) as given in Eq. (19).

$$\frac{\mathrm{d}T(t)}{\mathrm{d}t} = f\left(\Delta T(t)\right) \tag{19}$$

where $\Delta T(t)$ is the temperature difference between $T(t)$ and T_{amb} at time t.

3.4 Softening behavior

The softening phenomenon of VE material under large shear deformation was characterized by correcting the coefficients b and G in Eq. (7) as (Kasai *et al.*, 2001; Kasai and Tokoro, 2002)

$$b = b_{\mathrm{ref}} \lambda^{\alpha} \lambda_1 \tag{20}$$

$$G = G_{\mathrm{ref}} \lambda_2 \tag{21}$$

where b_{ref} and G_{ref} are the determined values of the coefficients b and G in Eq. (7) at T_{ref}; $\lambda_1 = 1 + C_1(\gamma_{\max} - 1)$; $\lambda_2 = 1 + C_2(\gamma_{\max} - 1)$; $\gamma_{\max}$ is the maximum shear strain; and C_1 and C_2 represent the slopes of b/b_{ref} versus $\gamma_{\max}$ and G/G_{ref} versus $\gamma_{\max}$, respectively.

Similarly, adopting the least squares method as given in Eq. (22), the value of the slope C_1 can be determined first. Then, with C_1 known, the value of the slope C_2 can be determined as given in Eq. (23).

$$\min\left\{\sum_{i=1}^{n}\left[\eta(b,\ \lambda\omega_i) - \eta_i\right]^2\right\} \tag{22}$$

$$\min\left\{\sum_{i=1}^{n}\left[G'(G,\ \lambda\omega_i) - G'_i\right]^2\right\} \tag{23}$$

where G'_i and η_i are the experimental shear storage modulus and loss factor of VE dampers under sinusoidal reversal loading with an angular frequency of ω_i at T_{amb}, respectively; and $\eta(b,\ \lambda\omega_i)$ and $G'(G,\ \lambda\omega_i)$ are calculated as per Eqs. (11) and (10), respectively, on the premise that the determined values of the coefficients b and G can satisfy Eqs. (22) and (23).

3.5 Hardening behavior

When VE material is deformed quickly (i.e. with a higher strain rate), its shear force response will be larger than with slow deformation (i.e. with a lower strain rate). This hardening phenomenon of VE material will become less significant when it has experienced larger shear deformation before, and has been described by putting an additional in-parallel spring with a nonlinear shear modulus G_h in the fractional derivative model, as given in Eq. (24) (Kasai *et al.*, 2001; Kasai and Tokoro, 2002).

$$G_h = \beta C_3 \min\left[\lambda\dot{\gamma}_{\max},\ 100\right] \tag{24}$$

where $\beta = \exp\left[C_4(\gamma_0 - 0.5)\right] \le 1$; C_3 and C_4 represent the slopes of G_h versus $\dot{\gamma}_{\max}$ and $\ln\beta$ versus $(\gamma_0 - 0.5)$, respectively; $\dot{\gamma}_{\max}$ is the maximum shear strain rate; and γ_0 is the experienced maximum shear strain.

4 Comparison between analytical predictions and experimental results

In this study, to describe the frequency-dependent behavior of the VE damper specimens, the values of the coefficients a, α, b, and G as introduced in Subsection 3.1 are determined as 2.47×10^{-17}, 0.62, 2.08, and 3.97 N/cm^2, respectively, by using the intermediate five-cycle test data of Specimen A under a maximum shear strain of 60% with excitation frequencies varying from 0.1 Hz to 5 Hz (a total of fifteen excitation frequencies were considered as listed in Table 1) and at an ambient temperature of 20°C, as listed in Table 3.

To characterize the ambient temperature-dependent property of the specimens, the values of the constants p_1 and p_2 as introduced in Subsection 3.2 are determined as 9.55 and 74.13 by using the intermediate five-cycle test data of Specimen A under a maximum shear strain of 60% with excitation frequencies varying from 0.1 Hz to 5 Hz (a total of fifteen excitation frequencies were considered as listed in Table 1) and at two ambient temperatures, 10°C and 40°C, as listed in Table 3.

In this study, the specific heat of the Type ISD111 VE material of the specimens is given as 187 N/(cm^2·°C). At the same ambient temperature in this study, the VE material layers subjected to a maximum shear strain of 300% definitely have the maximum temperature rise. Therefore, during cooling of the test at an ambient temperature of 20°C, the average temperature history measured by the ten thermocouples embedded in the two VE material layers of Specimen A is employed to determine a suitable higher-order polynomial function for describing the conduction and radiation of thermal energy within the VE material as introduced in Subsection 3.3 by using a curve-fitting procedure, as given in Eq. (25), shown in Fig. 7, and listed in Table 3.

Table 3 Identified coefficients, constants, slopes, and function in the analytical model

Excitation frequency effect	Coefficient			
	A	α	b	G
	2.47×10^{-17}	0.62	2.08	3.97 N/cm^2
Ambient temperature effect	Constant			
	p_1		p_2	
	9.55		74.13	
Temperature rise effect	Higher-order polynomial function of $\Delta T(t)$			
	$f(\Delta T(t))=(-1.04\times10^{-3})\Delta T^5(t)+(1.52\times10^{-2})\Delta T^4(t)-(7.98\times10^{-2})\Delta T^3(t)$ $+(1.77\times10^{-1})\Delta T^2(t)-0.17\Delta T(t)+0.038$			
Softening behavior	Slope			
	C_1		C_2	
	0.02		-0.05	
Hardening behavior	Slope			
	C_3		C_4	
	0.45 kN·s/cm^2		-0.15	

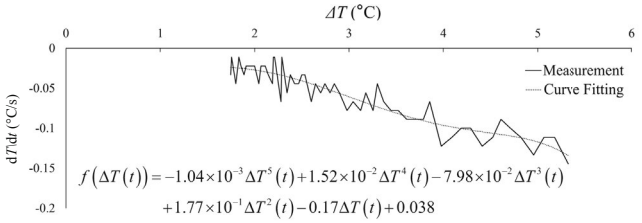

Fig. 7 Experimental and curve-fitting relation between temperature differences and temperature decreasing rates

$$f(\Delta T(t))=(-1.04\times10^{-3})\Delta T^5(t)+(1.52\times10^{-2})\Delta T^4(t)-(7.98\times10^{-2})\Delta T^3(t)+(1.77\times10^{-1})\Delta T^2(t)-0.17\Delta T(t)+0.038 \quad (25)$$

To describe the softening phenomenon of the specimens, the values of the slopes C_1 and C_2 as introduced in Subsection 3.4, as illustrated in Fig. 8, are determined as 0.02 and -0.05, respectively, by using the first cycle of the six-cycle test data of Specimen A under three maximum shear strains, 100%, 200%, and 300%, with excitation frequencies varying from 0.1 Hz to 5 Hz (a total of fifteen excitation frequencies were considered as listed in Table 1) and at an ambient temperature of 20°C, as listed in Table 3.

To explain the hardening phenomenon of the specimens, the differences between the maximum shear force responses at the beginning half cycle and the analytical predictions (without considering the hardening effect) of Specimen A under three maximum shear strains, 100%, 200%, and 300%, with excitation frequencies varying from 0.4 Hz to 1.5 Hz and at an ambient temperature of 20°C are employed to calculate the values of G_h at various values of $\dot{\gamma}_{\max}$ as introduced in Subsection 3.5. Accordingly, the value of C_3, the slope of G_h versus $\dot{\gamma}_{\max}$, as shown in Fig. 9(a), can be determined as 0.45 kN·s/cm^2 by a linear regression procedure, as listed in Table 3. Dividing the obtained values of G_h by the differences between the maximum shear force responses at the second half cycle and the analytical predictions (without considering the hardening effect) of Specimen A under maximum shear strains varying from 60% to 300% with excitation frequencies varying from 0.4 Hz to 5 Hz and at an ambient temperature of

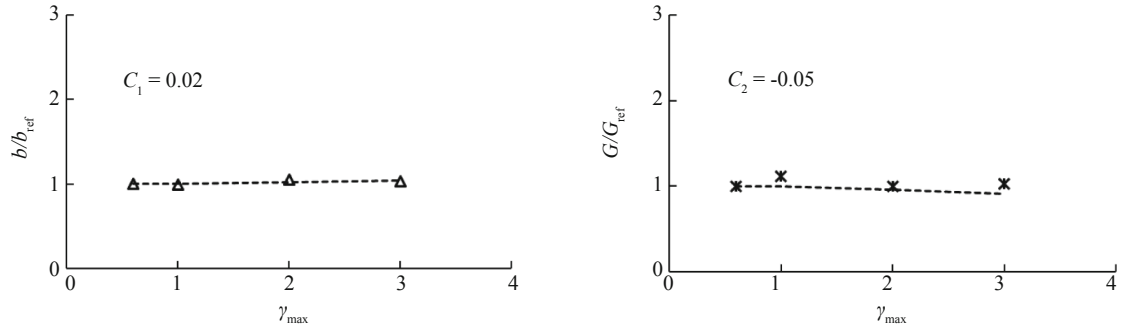

(a) b/b_{ref} versus $\gamma_{\max}$ (b) G/G_{ref} versus $\gamma_{\max}$

Fig. 8 Linear regression results when considering soften effect

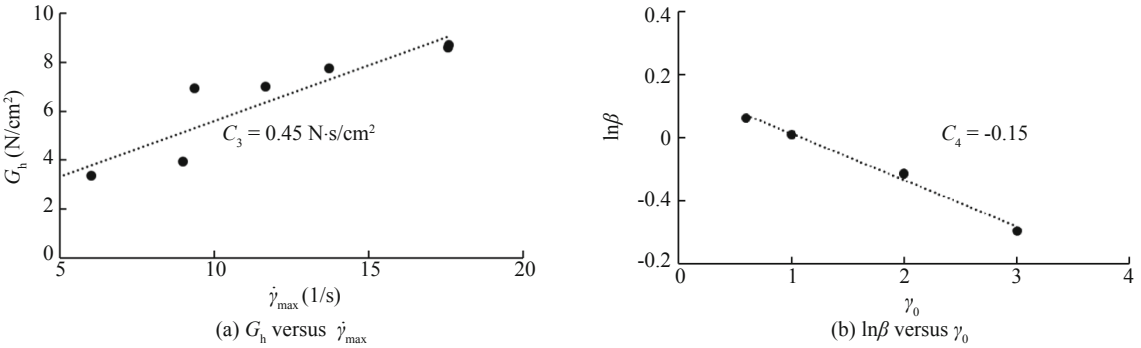

(a) G_h versus $\dot{\gamma}_{max}$ (b) lnβ versus γ_0

Fig. 9 Linear regression results when considering hardening effect

20°C, the values of β at various values of γ_0 can be determined. Taking a linear regression analysis on the values of $\ln\beta$ and $(\gamma_0 - 0.5)$, the value of C_4, i.e. the slope of $\ln\beta$ versus $(\gamma_0 - 0.5)$, as shown in Fig. 9(b), can be determined as -0.15, as listed in Table 3.

The comparisons between experimental force-displacement relation and prediction by the analytical model presented in Subsections 3.1 to 3.5 for the two specimens under maximum shear strains not greater than 300% with various excitation frequencies and at different ambient temperatures are shown in Figs. 10 to 12. To quantitatively evaluate the prediction accuracy, the coefficient of determination for force histories, R^2_{force}, and an author-defined energy dissipation ratio, *EDR*, are

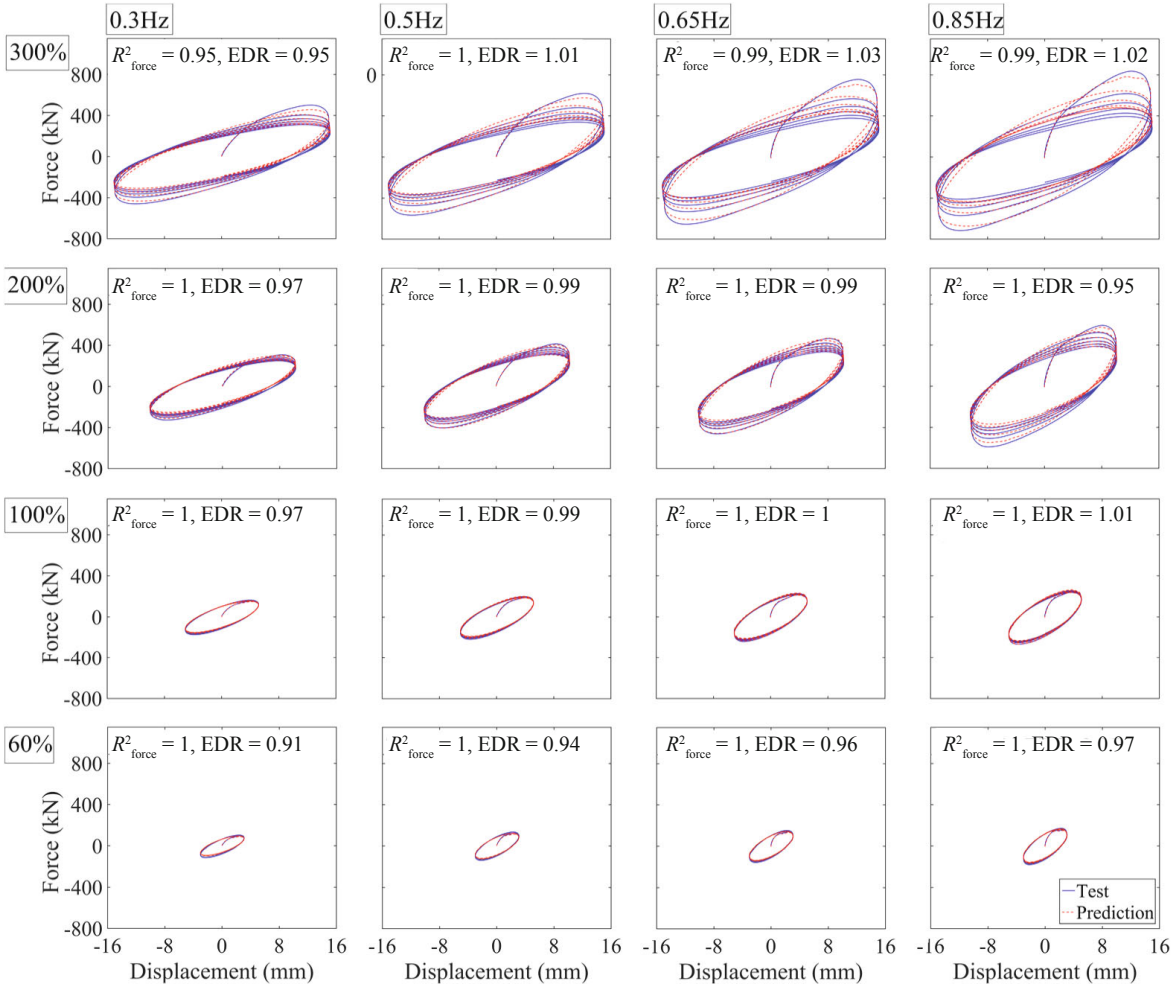

Fig. 10 Comparison of experimental results and analytical predictions of Specimen A under shear strains not greater than 300% with various excitation frequencies and at 20°C

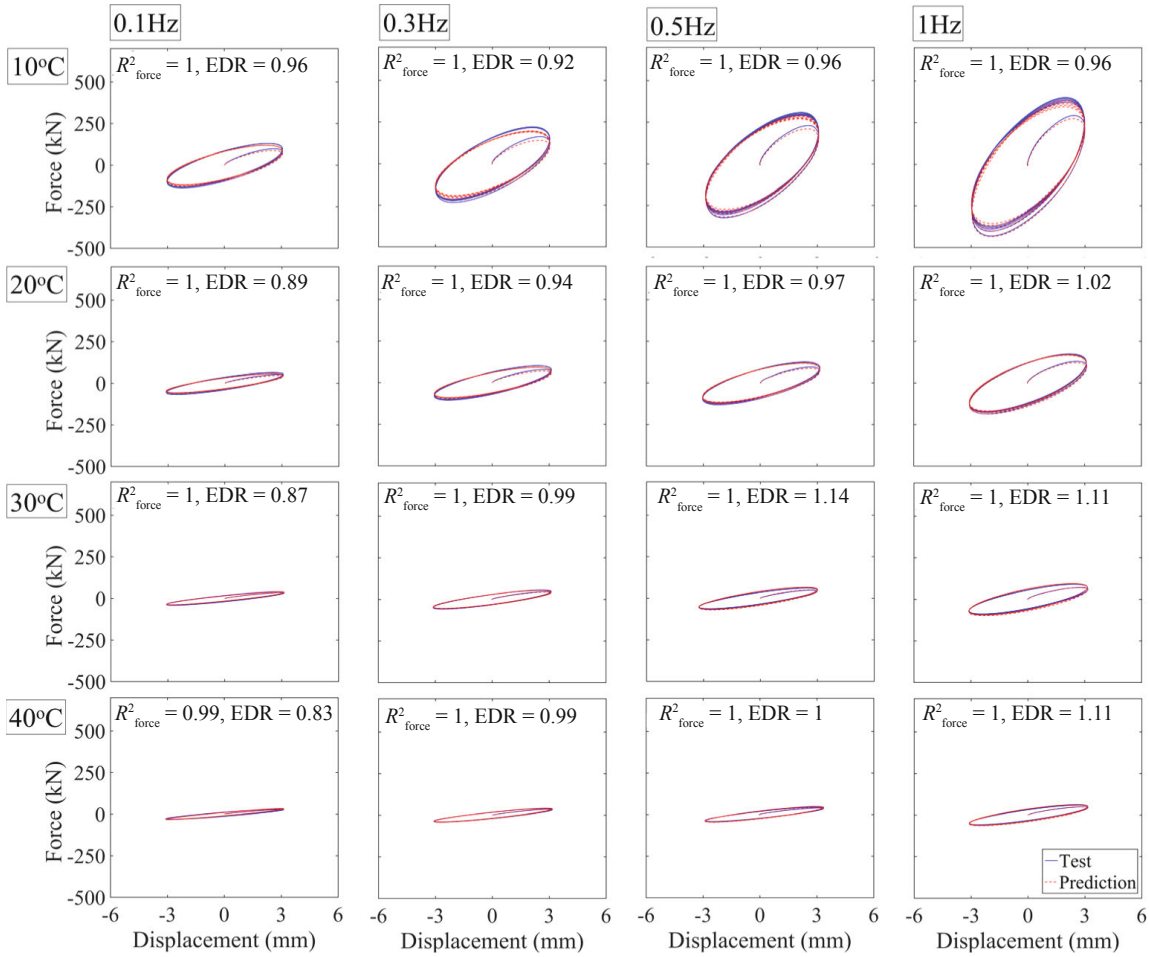

Fig. 11 Comparison of experimental results and analytical predictions of Specimen B under 60% shear strain with various excitation frequencies and at different ambient temperatures

calculated as per Eqs. (26) and (27), respectively, and are also provided in the figures. Note that the values of R^2_{force} and *EDR* closer to unity indicate that the prediction by the analytical model is more accurate.

$$R^2_{\text{force}} = 1 - \frac{\sum_{i=1}^{m}\left[\left(F_{\text{test}}\right)_i - \left(F_{\text{prediction}}\right)_i\right]^2}{\sum_{i=1}^{m}\left[\left(F_{\text{test}}\right)_i - \left(F_{\text{test}}\right)_{\text{mean}}\right]^2} \tag{26}$$

$$EDR = \frac{W_{D,\text{ prediction}}}{W_{D,\text{ test}}} \tag{27}$$

where $F_{\text{prediction}}$ and F_{test} are the predicted and experimental shear forces, respectively; the subscript i represents the data point at time t_i; the subscript "mean" represents the mean value of total data points during six cycles; m represents the total number of data points; and $W_{D,\text{ prediction}}$ and $W_{D,\text{ test}}$ are the predicted and experimental enclosed hysteresis loop areas, respectively.

As observed from the comparison shown in the figures, it is evident that adopting the analytical model together with considering the effects of frequencies, ambient temperatures, temperature rises, softening, and hardening, provides an excellent match with the test results of the full-scale VE damper specimens.

5 Conclusions

In this research, the design performance of full-scale VE dampers is experimentally and analytically investigated. Some conclusions are made as follows.

1. The test results of the full-scale VE damper specimens indicate that with the same displacement amplitude, the higher the excitation frequency (or strain rate), the larger the shear storage stiffness and the smaller the damping coefficient. In addition, the higher the ambient temperature, the smaller the shear storage stiffness and damping coefficient.

2. The temperature measure results during and after the six-cycle tests with different maximum shear strains,

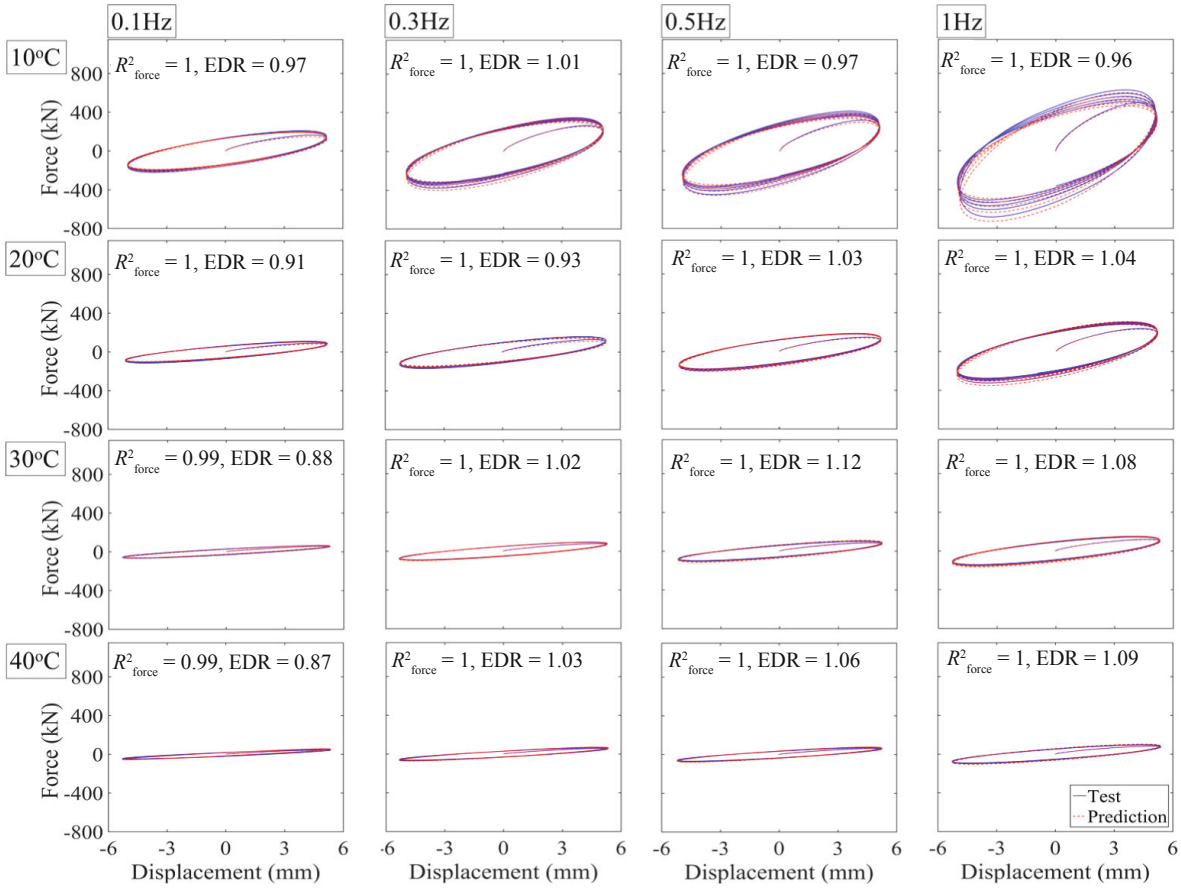

Fig. 12 Comparison of experimental results and analytical predictions of Specimen B under 100% shear strain with various excitation frequencies and at different ambient temperatures

excitation frequencies, and ambient temperatures show that the larger the hysteretic loop area, the higher the temperature rise within the VE material and a longer cooling time is needed. The measured ranges of temperature rises within the VE material during each test (10°C at most) and the cooling time after each test (5 minutes at most) are acceptable, and the temperature distribution contours in the VE material layers are reasonable for interpreting heat conduction and radiation.

3. The test results of the full-scale VE damper specimens show that with the same excitation frequency and at the identical ambient temperature, the shear force amplification at the beginning half cycle becomes more significant and is much larger than the nominal shear force capacity when subjected to a higher strain rate. This phenomenon, even if it might not significantly affect the overall structural seismic performance, should be seriously considered for the detailed design of connected members and structures.

4. By comparing the test results with the analytical predictions, it is demonstrated that adopting the analytical model based on the fractional derivative method together with considering the effects of frequencies, ambient temperatures, temperature rises, softening, and hardening can reproduce the experimental design performance of the full-scale VE damper specimens very well.

Acknowledgement

The study was financially supported by the Science and Technology Authority of Taiwan [107-2221-E-492-004-], and was experimentally supported by the Center for Research on Earthquake Engineering (NCREE), Applied Research Laboratories (NARL) of Taiwan and the Nippon Steel & Sumitomo Metal Corporation, Japan. This support is greatfully acknowledged.

References

Aprile A, Inaudi JA and Kelly JM (1997), "Evolutionary Model of Viscoelastic Dampers for Structural Applications," *Journal of Engineering Mechanics ASCE*, **123**(6).

Bagley RL and Torvic PJ (1983), "Fractional Calculus - a different approach to the analysis of viscoelastic damped structures. *AIAA Journal*, **21**(5): 741–748.

Bergman DM and Hanson RD (1993), "Viscoelastic Mechanical Damping Devices Tested at Real Earthquake

Displacements," *Earthquake Spectra*, **9**(3): 389–417.

Chang KC, Soong TT, Oh ST and Lai ML (1992), "Effect of Ambient Temperature on Viscoelastically Damped Structure," *Journal of Structural Engineering*, *ASCE* , **118**(7): 1955–1973.

Chang KC, Soong TT, Lai ML and Nielsen EJ (1993), "Viscoelastic Dampers as Energy Dissipation Devices for Seismic Applications," *Earthquake Spectra*, **9**(3): 371–387.

Chang TS and Singh MP (2009), "Mechanical Model Parameters for Viscoelastic Dampers," *Journal of Engineering Mechanics*, **135**(6): 581–584.

De Lima AMG, Rade DA, Lacerda HB and Araújo CA (2015), "An Investigation of the Self-Heating Phenomenon in Viscoelastic Materials Subjected to Cyclic Loadings Accounting for Prestress," *Mechanical Systems and Signal Processing*, **58-59**: 115–127.

Federal Emergency Management Agency FEMA273 (1997), *NEHRP Guidelines and Commentary for the Seismic Rehabilitation of Buildings*, Building Seismic Safety Council: Washington, DC, U.S.A.

Gandhi F and Chopra I (1996), "A Time-Domain Non-Linear Viscoelastic Damper Model," *Smart Materials and Structures*, **5**(5): 517–528.

Gemant A (1936), "A Method of Analyzing Experimental Results Obtained from Elasto-Viscous Bodies," *Journal of Applied Physics*, **7**(8): 311–317.

Ghobarah A (2001), "Performance-Based Design in Earthquake Engineering: State of Development," *Engineering Structures*, **23**(8): 878–884.

Kasai K and Tokoro K (2002), "Constitutive Rule for Viscoelastic Materials Considering Temperature, Frequency, and Strain Sensitivities (part 2)," *Journal of Structural and Construction Engineering*, Architectural Institute of Japan, **561**: 55–63.

Kasai K, JA Munshi, Lai ML and Maison BF (1993), "Viscoelastic Damper Hysteretic Model: Theory, Experiment, and Application," *Proceedings of ATC-17-1 Seminar on Seismic Isolation, Passive Energy Dissipation, and Active Control*, Applied Technology Council, San Francisco California, **2**: 521–532.

Kasai K, Teramoto M, Okuma K and Tokoro K (2001), "Constitutive Rule for Viscoelastic Materials Considering Temperature, Frequency, and Strain Sensitivities (part 1)," *Journal of Structural and Construction Engineering*, Architectural Institute of Japan, **543**: 77–86.

Lai ML, Chang KC, Soong TT, Hao DS and Yeh YC (1995), "Full-Scale Viscoelastially Damped Steel Frame," *Journal of Structural Engineering*, *ASCE*, **121**(10): 1443–1447.

Lewandowski R and Chorążyczewski B (2010), "Identification of the Parameters of the Kelvin–Voigt and the Maxwell Fractional Models, Used to Modeling of Viscoelastic Dampers," *Computers and Structures*, **88**(1-2): 1–17.

Mahmoodi P, Robertson LE, Yontar M, Moy C and Feld I (1987), "Performance of Viscoelastic Dampers in World Trade Center Towers. Dynamic of Structures," *Proceedings of Sessions at Structural Congress 87*, Orlando, Florida, 1987.

Nippon Steel & Sumitomo Metal Corporation. *http://www.nssmc.com/*.

Park SW (2001), "Analytical Modeling of Viscoelastic Dampers for Structural and Vibration Control," *International Journal of Solids and Structures*, **38**(44-45): 8065–8092.

Samali B and Kwok KCS (1995), "Use of Viscoelastic Dampers in Reducing Wind- and Earthquake-Induced Motion of Building Structures," *Engineering Structures*, **17**(9): 639–654.

Shen KL and Soong TT (1995), "Modeling of Viscoelastic Dampers for Structural Applications," *Journal of Engineering Mechanics ASCE*, **121**(6).

Skilling JB, Tschanz T, Isyumov N, Loh P and Devenport AG (1986), "Experimental Studies, Structural Design and Full-Scale Measurements for the Columbia Seafirst Centre," *Proceedings of Building Motion in Wind, ASCE Convention*, Seattle, Washington, 1986.

Soong TT and Spencer Jr BF (2002), "Supplemental Energy Dissipation: State-of-the-Art and State-of-the-Practice," *Engineering Structures*, **24**(3): 243–259.

Wang SJ, Chang KC, Hwang JS, Huang YN, Lin WC and Yang CY (2017), "Recent Progress in Taiwan on Seismic Isolation, Energy Dissipation, and Active Vibration Control," *Proceedings of New Zealand Society for Earthquake Engineering* (*NZSEE*) *Annual Conference and Anti-seismic Systems International Society* (*ASSISi*) *15th World Conference on Seismic Isolation, Energy Dissipation, and Active Vibration Control of Structures*, Wellington, New Zealand, 2017.

Xu ZD, Xu C and Hu J (2015), "Equivalent Fractional Kelvin Model and Experimental Study on Viscoelastic Damper," *Journal of Vibration and Control*, **21**(13): 2536–2552.